The Astronomical Journal, 123:1039–1049, 2002 February

FROM KUIPER BELT OBJECT TO COMETARY NUCLEUS: THE MISSING ULTRARED MATTER

David C. Jewitt
Institute for Astronomy, University of Hawaii at Manoa, 2680 Woodlawn Drive, Honolulu, HI 96822
Received 2001 September 26; accepted 2001 November 14

ABSTRACT

We combine new and published data to show that the optical color distributions of cometary nuclei and Kuiper belt objects (KBOs) are significantly different. The nuclei are, as a group, bluer than the KBOs, indicating that the surface chemical and/or physical properties of the two types of bodies are different. Objects in the dynamically intermediate Centaur class have optical colors like those of KBOs, while the color distribution of candidate dead comets is indistinguishable from that of the cometary nuclei. We infer that the surfaces of KBOs are modified upon entry to the inner solar system. We consider several mechanisms and conclude that the color change is most likely caused by the rapid burial of ancient surface materials exposed in the Kuiper belt. The distinctive, ultrared material that is present on the surfaces of some KBOs is absent on the cometary nuclei.

Key words: comets: general — Kuiper belt — minor planets, asteroids

1. INTRODUCTION

The lifetimes of comets when near the Sun are limited by sublimation and by strong gravitational encounters with the planets. The sublimation and dynamical lifetimes ($\sim 10^4$ and $\sim 4.5 \times 10^5$ yr, respectively; Levison & Duncan 1994) are both very short compared with the 4.5×10^9 yr age of the solar system. For this reason, it has long been recognized that the observed comets must be resupplied from a more distant, longer-lived source if their population is to be maintained in a steady state. Long-period comets (periods $\geq$200 yr) originate in the Oort cloud (Oort 1950). A majority of the short-period comets (excluding the Halley-type comets, whose large, inclined orbits suggest capture from the long-period population) originate in the region beyond Neptune, frequently called the Kuiper belt (Fernández 1980; Duncan, Quinn, & Tremaine 1988).

Given their likely source, it seems natural to expect that the cometary nuclei should closely resemble their trans-Neptunian parents. The optical properties (albedos, colors) of comets and Kuiper belt objects (KBOs), for example, should be similar. In fact, this is the basis for the diameter determinations of almost all KBOs made to date: the diameters are determined from optical photometry under the assumption that the KBOs possess comet-like geometric albedos (typically 0.04). However, this remains an assumption, and a systematic comparison of the cometary nuclei with the KBOs has not yet been presented.

Observations of most cometary nuclei are challenging, and few reliable data exist. When near the Sun, the nuclei are surrounded by comae that photometrically can swamp the signal from the nucleus. When far from the Sun, the coma is diminished (and may be absent), but the nucleus then appears very faint and is difficult to measure. For these reasons, studies of cometary nuclei have focused on objects whose intrinsic outgassing activity is very low even when at perihelion (P/Arend-Rigaux, P/Neujmin 1, P/Encke, and P/Tempel 2 are classic examples). In these objects, the nucleus is unmistakable even though it may sometimes be attended by an adjacent, low surface brightness coma. High-resolution observations of more active comets with the *Hubble Space Telescope* (*HST*) have been used to extract the signals of a number of cometary nuclei by P. Lamy and collaborators (Lamy et al. 1998, 1999).

The surfaces of some KBOs and Centaurs show very red colors (see, e.g., Luu & Jewitt 1996; Tegler & Romanishin 2000; Barucci et al. 2001; Jewitt & Luu 2001), widely thought to indicate processing of the surface materials by prolonged cosmic-ray bombardment of organics (Johnson et al. 1987; Wilson, Sagan, & Thompson 1994; Cruikshank et al. 1998). Previous work has hinted that the comets may differ from other solar system objects. In particular, Luu & Jewitt (1996) compared the optical colors of KBOs and cometary nuclei and found that the comets lacked the red colors of the KBOs. However, with only 11 KBOs and six cometary nuclei in their sample, this conclusion cannot be considered robust. In this paper, we compare the optical colors of larger samples of nuclei and KBOs, taking advantage of recent improvements in observations of objects in both classes. We extend this comparison to the Centaurs (dynamical precursors to the comets) and to candidate dead comets (the likely end states).

2. OBSERVATIONS

New observations of cometary nuclei and candidate dead comets were taken at the University of Hawaii 2.2 m telescope on Mauna Kea. A Tektronix CCD detector having 2048×2048 pixels was mounted at the f/10 Cassegrain focus. The image scale on the detector was $0\farcs219$ pixel^{-1}, giving a field of view of $7' \times 7'$. The bias level was determined for each image using the overclock region. We used images of the twilight sky and median-stacked data frames to construct flat-field images with which to correct for sensitivity variations among the pixels.

Observations were taken under photometric conditions and with median seeing conditions of $0\farcs75$ FWHM. We used broadband *BVRI* filters, close in shape to the Kron-Cousins photometric system. Absolute calibration was obtained using observations of stars from Landolt (1992). Short integration times were used to limit the trailing of images with respect to background stars. A journal of observations is given in Table 1. The photometric results are listed in Table 2.

TABLE 1
JOURNAL OF OBSERVATIONS

Object	UT Date	R[a] (AU)	Δ[b] (AU)	α[c] (deg)
2P/Encke	1996 Aug 16.4927	3.268	2.493	13.1
	1999 Sep 12.5167	3.651	2.650	1.9
6P/d'Arrest	2001 Jun 17.3166	2.667	2.320	22.1
95P/Chiron	2000 Jul 1.4125	9.867	10.363	4.8
143P/Kowal-Mrkos	2001 Jun 19.4550	3.400	2.471	8.2
1996 PW	1996 Aug 16.4200	2.537	1.531	3.4
1999 LE_{31}	2000 Jul 2.3141	5.267	5.312	11.0
2000 HE_{46}	2000 Jul 2.2725	2.562	2.691	22.1

[a] Heliocentric distance.
[b] Geocentric distance.
[c] Phase angle.

3. DISCUSSION OF THE SAMPLE

It is useful to parameterize the spectra using the normalized reflectivity gradient, S' [% (1000 Å)$^{-1}$]:

$$S' = (dS/d\lambda)/\bar{S}\,, \quad (1)$$

in which S is the reflectivity (object flux density divided by the flux density of the Sun at the same wavelength λ) and $\bar{S}$ is the mean value of the reflectivity in the wavelength range over which $dS/d\lambda$ is computed. The gradient S' is used to express the percentage change in the strength of the continuum per 1000 Å of wavelength difference. It is clearly a simplistic measure, but one that is adequate to the task, since most reflection spectra are linear across the visible wavelengths. Our data consist of a mixture of spectra and broadband filter colors. When colors are available, we choose the m_V–m_R color index to study the color distributions, since this index is available for the largest number of KBOs, Centaurs, and related bodies. S' can be related to the m_V–m_R color through

$$m_V - m_R = (m_V - m_R)_\odot + 2.5\log\left(\frac{2 + S'\Delta\lambda}{2 - S'\Delta\lambda}\right), \quad (2)$$

(Luu & Jewitt 1990b), in which m_V–m_R is the color of the object, $(m_V$–$m_R)_\odot$ is the color of the Sun [$(m_V$–$m_R)_\odot = 0.36$ in the Kron-Cousins system], S' [% (1000 Å)$^{-1}$] is the normalized spectral gradient, and $\Delta\lambda$ is the difference between the V- and R-band center wavelengths. We take $\Delta\lambda = 1000$ Å.

3.1. *Cometary Nuclei*

Observations from the present work and from the published literature are summarized in Tables 3 and 4. For the cometary nuclei, we have listed only objects for which a clear case exists that the coma-free nucleus has been detected. Evidence that the nucleus has been directly detected includes one or more of (1) the measurement of a periodic rotation curve (comets Encke, Tempel 2, Neujmin 1, Wirtanen, Arend-Rigaux, Chiron, and Kowal-Mrkos), (2) the absence of measurable coma in ultradeep imaging observations (Encke, d'Arrest, Tempel 2, Grigg-Skjellerup, Wilson-Harrington, Arend-Rigaux, and Kowal-Mrkos), and (3) isolation of a pointlike source in the presence of weak coma (as with *HST* observations of P/Honda-Mrkos-Pajdušáková and P/Wirtanen and ground-based observations of P/Tempel 2, Giacobini-Zinner, Neujmin 1, Arend-Rigaux, and Chiron). In several cases, rotational light curves are detected both in the absence of coma (when far from perihelion) and in the presence of coma (when nearer perihelion).

The colors of the nuclei are summarized in Table 3. In the table, we have listed both m_V–m_R colors and spectral gradients S', for convenience. Colors (spectral gradients) listed in parentheses are calculated from spectral gradients (colors) that were directly measured. The spectra of candidate dead comets, Table 4, are treated exactly the same as the comets and need no further explanation. We briefly discuss each of the nucleus entries in Table 3.

1P/Halley.—The orbit of this comet has Tisserand parameter $T_J = -0.6$, indicating that it is probably not derived from the Kuiper belt. Therefore we do not include it in the following analysis, but we mention its properties because of its special status in having been studied at close range by passing spacecraft and, so, in providing a context for the interpretation of data from nuclei observed remotely. Images show an elongated body $8 \times 8 \times 16$ km in size with outgassing from a small number of active areas occupying a fraction (~20%) of the nuclear surface. The geometric albedo of the surface away from the vents is estimated at $p \sim 0.03$, while multifilter photometry from *Giotto* gives $S' = 6\% \pm 3\%$ per 1000 Å (Thomas & Keller 1989), implying a nearly neutral reflection spectrum. Ground-

TABLE 2
NEW COLOR PHOTOMETRY

Object	UT Date	m_R	m_B–m_V	m_V–m_R	m_R–m_I
2P/Encke	1996 Aug 16.4927	19.43 ± 0.03	...	0.43 ± 0.05	0.38 ± 0.04
	1999 Sep 12.5167	19.14 ± 0.05	...	0.38 ± 0.06	0.45 ± 0.06
6P/d'Arrest	2001 Jun 17.3166	20.88 ± 0.02	0.78 ± 0.04	0.54 ± 0.04	0.45 ± 0.04
95P/Chiron	2000 Feb 1.4125	16.29 ± 0.01	...	0.31 ± 0.02	0.37 ± 0.02
143P/Kowal-Mrkos	2001 Jun 19.4550	18.54 ± 0.02[a]	0.84 ± 0.02	0.58 ± 0.02	0.55 ± 0.02
	2001 Jun 19.4983	18.49 ± 0.02[a]	0.80 ± 0.02	0.58 ± 0.02	0.57 ± 0.02
1996 PW	1996 Aug 16.4200	16.99 ± 0.03	...	0.54 ± 0.05	0.54 ± 0.04
1999 LE_{31}[b]	2000 Jul 2.3141	20.44 ± 0.05	0.87 ± 0.06	0.55 ± 0.07	0.40 ± 0.06
2000 HE_{46}	2000 Jul 2.2725	20.11 ± 0.02	0.74 ± 0.07	0.51 ± 0.05	0.49 ± 0.05

[a] The R magnitude was evaluated at the epoch of each filter measurement, to correct for the large rotational light curve of this object. The listed magnitude applies only to the listed time of observation.
[b] Possible cirrus in this photometry sequence.

TABLE 3
COLORS OF COMETARY NUCLEI

Object	λ_1, λ_2[a]	S'	m_V-m_R	Ref.
1P/Halley	4400–8100	6 ± 3	(0.43 ± 0.03)	1
2P/Encke	4400–7200	11 ± 2	(0.48 ± 0.02)	2
	VR	(6.5 ± 3.5)	0.43 ± 0.05	3
		(2.0 ± 4.5)	0.38 ± 0.06	3
6P/d'Arrest	*VR*	(16.5 ± 3.5)	0.54 ± 0.04	3
10P/Tempel 2	*VR*	(16 ± 3)	0.53 ± 0.03	4
	4400–7200	20 ± 3	(0.58 ± 0.03)	5
21P/Giacobini-Zinner	3800–6300	12.8 ± 2.0	(0.50 ± 0.02)	6
26P/Grigg-Skjellerup	*VR*	(-13 ± 8)	0.42 ± 0.10[b]	7
28P/Neujmin 1		(8.5 ± 4.5)	0.45 ± 0.05	4
		(13 ± 4)	0.50 ± 0.04	4
	VR	(8.5 ± 4.5)	0.45 ± 0.05	8
107P/Wilson-Harrington	4000–6000	-5 ± 3	(0.31 ± 0.03)	9
45P/Honda-Mrkos-Pajdušáková	5500–6500	10 ± 10	(0.47 ± 0.10)	10
46P/Wirtanen	5500–6500	10 ± 7	(0.47 ± 0.07)	11
49P/Arend-Rigaux	*VR*	(10 ± 1)	0.47 ± 0.01	12
	3800–6300	10.1 ± 0.6	(0.47 ± 0.01)	6
95P/Chiron	3800–6300	-3.2 ± 0.2	(0.32 ± 0.01)	6
	VR	(7.5 ± 2.0)	0.44 ± 0.02	3
		(-4.5 ± 2.0)	0.31 ± 0.02	3
143P/Kowal-Mrkos	*VR*	(21 ± 2)	0.58 ± 0.02	3

NOTE.—Numbers in parentheses are derived from numbers not in parentheses.
[a] Wavelength range used to compute S'. *VR* indicates that the primary measurement used filters.
[b] Johnson filter system employed; see text.
REFERENCES.—(1) Thomas & Keller 1989; (2) Luu & Jewitt 1990a; (3) this work; (4) Jewitt & Meech 1988; (5) Jewitt & Luu 1989; (6) Luu 1993; (7) Boehnhardt et al. 1999; (8) Delahodde et al. 2001; (9) Chamberlin et al. 1996; (10) Lamy et al. 1999; (11) Lamy et al. 1998; (12) Millis et al. 1988.

based observations provide a Thuan-Gunn color index $g-r \approx V-R = 0.3 \pm 0.1$ (Jewitt & Danielson 1984), which is consistent with the spacecraft value.

2P/Encke.—The nucleus of this low-activity comet has been detected at radar wavelengths (Kamoun et al. 1982) and studied photometrically in the optical and thermal infrared, resulting in the determination of a 15.08 ± 0.08 hr rotation period, axis ratio $\sim 1.8:1$ (Jewitt & Meech 1987; Luu & Jewitt 1990a), and a nucleus albedo $p_R = 0.05 \pm 0.02$ (Fernández et al. 2000). Measurements of the nucleus color include a CCD spectrum (Luu & Jewitt 1990a) and broadband photometry (Table 3). The broadband colors are both bluer than the spectrum by about $2\,\sigma$ (Table 2). This could be a rotational variation or, more likely, a reflection of the difficulty of measurement of the spectrum of this faint object. The weighted mean color

TABLE 4
COLORS OF CANDIDATE DEAD COMETS

Object	λ_1, λ_2	S'	m_V-m_R	Ref.
944 Hidalgo[a]	3800–6300	6.8 ± 0.3	(0.43 ± 0.01)	1
2201 Oljato	5500–7000	4.0 ± 1.7	(0.40 ± 0.02)	2
	4000–6000	0 ± 3	(0.36 ± 0.03)	3
2212 Hephaistos	4400–7200	5.0 ± 1.0	(0.41 ± 0.01)	1
3200 Phaethon	5500–7000	-1.8 ± 0.7	(0.34 ± 0.01)	2
	4400–7200	-13.3 ± 1.0	(0.22 ± 0.01)	1
	4000–6000	0 ± 2	(0.36 ± 0.02)	3
3552 (1983 SA)	3800–6300	2.4 ± 1.0	(0.39 ± 0.01)	1
1992 LC	5500–7000	3.0 ± 1.0	(0.39 ± 0.01)	2
1995 QU_3	5500–7000	6.4 ± 2.8	(0.43 ± 0.03)	2
1996 PW	4000–9000	11.3 ± 1.5	(0.48 ± 0.02)	4
	VR	(16.5 ± 4.0)	0.54 ± 0.05	5
1997 SE_5	4000–9000	6.0 ± 0.9	(0.43 ± 0.01)	4
1998 WU_{24}	*VR*	(15.5 ± 4.0)	0.53 ± 0.04	6
1999 LE_{31}	*VR*	(18 ± 7)	0.55 ± 0.07	5
2000 HE_{46}	*VR*	(14 ± 5)	0.51 ± 0.05	5

NOTE.—Numbers in parentheses are derived from numbers not in parentheses.
[a] Weighted mean of several measurements given in the reference.
REFERENCES.—(1) Luu 1993; (2) Hicks, Fink, & Grundy 1998; (3) Chamberlin et al. 1996; (4) Hicks et al. 2000; (5) this work; (6) Davies et al. 2001.

is $S' = 8.9\% \pm 1.6\%$ per 1000 Å, corresponding to $m_V - m_R = 0.46 \pm 0.02$.

6P/d'Arrest.—We observed comet d'Arrest on UT 2001 June 16–17 when at heliocentric distance $R = 2.67$ AU (Tables 1 and 2). It appeared completely stellar in 0.″7 seeing, even in shift-added images with total integrations of 2000 s. The point source had absolute magnitude $m_V(1, 1, 0) = 16.58$. Time-resolved measurements of the light curve will be reported in a separate paper. Comet d'Arrest was also observed in the presence of coma by Fay & Wisniewski (1978) when at $R = 1.168$ AU. They reported a neutral nucleus color ($m_V - m_R = 0.58 \pm 0.13$ in a system where the solar color is $m_V - m_R = 0.55$) that is different from the one found in the present data. However, they used a large photometric aperture and their reported absolute magnitude, $m_V(1, 1, 0) = 14.6 \pm 0.05$, is brighter than in our data by 2 mag, leading us to believe that their measurements were contaminated by a substantial coma contribution.

10P/Tempel 2.—This low-activity comet was studied intensively at the 1989 apparition, resulting in the photometric isolation of the nucleus and the determination of the rotational light curve (period 8.95 ± 0.01 hr; Jewitt & Luu 1989), nucleus geometric albedo (0.03 ± 0.01), and size ($16 \times 9 \times 9$ km; A'Hearn et al. 1989; Campins et al. 1995). The absolute magnitude is $m_R(1, 1, 0) = 13.6 \pm 0.1$. The color has been measured both in the absence of coma, at $R = 3.99$ AU (Jewitt & Meech 1988), and with faint coma present (Jewitt & Luu 1989). From spectroscopic observations, the nucleus was found to be redder ($S' = 20\% \pm 3\%$ per 1000 Å) than the adjacent dust coma ($S' = 1\% \pm 3\%$ per 1000 Å). The photometric and spectroscopic determinations of S' are in agreement, within the uncertainties. Both show a nucleus that is considerably redder than sunlight.

21P/Giacobini-Zinner.—The nucleus was observed spectroscopically at $R = 3.5$ AU on UT 1992 May 21 (Luu 1993). No resolved coma was visible, and no spectral lines of gases in the coma were evident. The apparent magnitude was $m_V = 20.9 \pm 0.2$ [$m_V(1, 1, 0) = 15.8 \pm 0.1$].

26P/Grigg-Skjellerup.—Boehnhardt et al. (1999) observed this comet 1 year past perihelion when at 3.82 AU heliocentric distance. A combined 9.5 hr integration showed a starlike (point source) image with no evidence of coma down to a surface brightness limit of 27 mag arcsec^{-2}. The $m_V - m_R$ color was 0.42 ± 0.10, in a system in which the color of the Sun is $(m_V - m_R)_\odot = 0.55$. Relative to the Sun, the nucleus is slightly blue, although not significantly so in view of the large measurement uncertainty. Boehnhardt et al. also observed P/Schwassmann-Wachmann 3 and reported a nucleus detection with $m_V - m_R = 0.48 \pm 0.17$ in the same photometric system. In view of the coma contamination evident in their Figure 2 and the lack of complementary supporting evidence, however, we elect not to include the P/Schwassmann-Wachmann 3 data in our nucleus sample.

28P/Neujmin 1.—Optical observations of this very low activity object have been secured over a range of heliocentric distances 3.9 AU $< R <$ 10.5 AU (Jewitt & Meech 1988; Delahodde et al. 2001). Except near perihelion, it appears as a point-source object even in deep imaging observations. The rotational light curve of the nucleus is clearly identified (period 12.76 ± 0.03 hr, range 0.45 ± 0.05 mag, corresponding to axis ratio 1.5 : 1). Simultaneous thermal and optical observations yield a geometric albedo $p_R = 0.03 \pm 0.01$ (Campins, A'Hearn, & McFadden 1987; Campins et al. 1995).

45P/Honda-Mrkos-Pajdušáková.—Lamy et al. (1999) used the high angular resolution of *HST* to isolate the nucleus in this weakly active comet (dust mass-loss rate $Q_d \sim 1$ kg s^{-1}). Observed when at $R = 0.96$ AU, the nucleus reflectivity was found to be slightly redder than solar ($S' = 10\% \pm 10\%$ per 1000 Å) in the *VR* region of the spectrum. The spectrum showed a downturn toward short wavelengths but is linear across the *V*–*R* wavelength range considered here. The spectrum of the coma adjacent to the nucleus was completely different, with a strong upturn (Rayleigh scattering?) at short wavelengths.

46P/Wirtanen.—This comet was observed photometrically at $R = 2.45$ AU using *HST* (Lamy et al. 1998). The comet was weakly active (estimated dust mass-loss rate $Q_d \sim 4$ kg s^{-1}), but the high angular resolution of *HST* enabled isolation of the nuclear signal. The rotation period of the nucleus was found to be 6.0 ± 0.3 hr and the photometric range 0.2 mag. The nucleus is moderately red ($S' = 10\% \pm 7\%$ per 1000 Å).

49P/Arend-Rigaux.—This object is well known as a short-period comet of intrinsically low activity. Except near perihelion, the comet is usually recorded as having an asteroidal appearance. The nucleus has been photometrically isolated and the rotational light curve determined: the period is 13.47 ± 0.02 hr (Jewitt & Meech 1985; Millis, A'Hearn, & Campins 1988). Simultaneous optical/infrared observations yielded an albedo $p_R = 0.04 \pm 0.01$ and a prolate ellipsoidal shape with axes $13 \times 8 \times 8$ km (Millis et al. 1988; Campins et al. 1995). The optical color of the nucleus was measured using filters when at $R = 1.5$ AU by Millis et al. (1988) and spectroscopically at $R = 2.18$–2.36 AU by Luu (1993). These independent color measurements are in excellent agreement (Table 2).

95P/Chiron.—Originally classified as the prototypical Centaur, this object displays a faint coma and is thus, by definition, also a comet. At brightness maximum in the late 1980s ($R \sim 12$ AU), the integrated dust cross section in the coma of Chiron rivaled the scattering cross section of the nucleus (Luu & Jewitt 1990c; Meech & Belton 1990). Since then the integrated, intrinsic brightness has decreased by more than a factor of 2. Periodic (~6 hr) brightness variations in the central region clearly show the dominance of the nucleus in the scattering cross section. The nucleus has also been detected thermally, in the mid-infrared (Campins et al. 1994) and submillimeter (Altenhoff & Stumpff 1995) wavelength regimes.

107P/Wilson-Harrington = 4015 = 1979 VA.—This object exhibits such low activity that it has been misclassified as an asteroid. The surface is dark (geometric albedo calculated from the isothermal latitude model is $p = 0.05 \pm 0.01$), and the effective radius is small (2.0 ± 0.3 km; Campins et al. 1995). A spectrum of the point-source nucleus was presented by Chamberlin et al. (1996). The spectral slope listed in Table 3 was estimated by eye from the reflectivity spectrum plotted in their Figure 1.

143P/Kowal-Mrkos.—We observed this comet UT 2001 June 18–20 and 28–30 (Table 1). A large, periodic modulation of the brightness was observed in all data and interpreted as the rotational light curve of the bare nucleus (the light curve will be the subject of a separate paper). This interpretation is buttressed by the complete absence of coma in P/Kowal-Mrkos, even in shifted, co-added images from

TABLE 5
MEAN COLORS

Group	S'_{min} [a]	S'_{max} [a]	S'_m [a]	$S' \pm \sigma$	$m_V - m_R$	n [b]	Ref.
Dead comets ...	−6	18	6	7.2 ± 2.0	0.44 ± 0.02	12	1
Nuclei	−13	21	10	8.3 ± 2.8	0.45 ± 0.02	12	1
D-types	3	13	9	8.8 ± 0.5	0.45 ± 0.01	19	2
Trojans	3	25	9	9.6 ± 0.9	0.46 ± 0.01	32	3
Centaurs	1	39	10	17 ± 5	0.54 ± 0.07	9	4
KBOs.....	2	40	25	22.9 ± 1.7	0.61 ± 0.01	28	5

NOTE.—Listed uncertainties are the standard errors on the means of N measurements.
[a] S'_{min}, S'_{max}, and S'_m are respectively the minimum, maximum, and median values of S' within each group.
[b] Number of objects in the group.
REFERENCES.—(1) This work; (2) Fitzsimmons et al. 1994; (3) Jewitt & Luu 1990; (4) colors compiled by Barucci et al. 2001 and Peixinho et al. 2001; (5) Jewitt & Luu 2001.

data taken over many hours. We also measured the broadband colors of P/Kowal-Mrkos (Table 2). This object passed only 0.16 AU from Jupiter in 1989 March (Marsden 2000), an event that raised its perihelion from 1.9 to 2.5 AU. The resulting lower mean surface temperature is perhaps responsible for the lack of observable cometary activity.

3.2. *Dead Comets*

The median dynamical lifetimes of short-period comets are greater than the sublimation lifetimes, leading to the conclusion that dead comets should be abundant. These objects would possess dynamical similarities to active comets but, lacking distinguishing comae, would be difficult to identify using only physical observations. Recently, albedo measurements of near-Earth objects (NEOs) have revealed a link between surface albedo and dynamical properties (measured by the Tisserand parameter, with respect to Jupiter). Specifically, asteroidal-appearing objects in comet-like orbits have comet-like (low) albedos. In contrast, low albedos are rare among the asteroidal-appearing NEOs with asteroid-like Tisserand parameters (Fernández, Jewitt, & Sheppard 2001). Table 4 lists spectral measurements of NEOs in predominantly comet-like orbits. These objects show a remarkable concordance with the color distribution of the cometary nuclei. The mean colors [S'(nuclei) $= 8.3\% \pm 2.8\%$ per 1000 Å, S'(dead comets) $= 7.2\% \pm 2.0\%$ per 1000 Å] are consistent. Both populations include blue ($S' < 0$) members that are very rare or not seen among other groups of objects. The color distributions of the nuclei and the candidate dead comets are formally indistinguishable.

3.3. *Other Objects*

We define Centaurs as objects with perihelia outside Jupiter's orbit and semimajor axes smaller than Neptune's (Jewitt & Kalas 1998). Some Centaurs (2060 = 95P/Chiron, P/Schwassmann-Wachmann 1, and P/Oterma) are outgassing and so are also classified as comets. Most appear stellar in all observations to date. Their important feature is that they are strongly interacting with the gas-giant planets and therefore possess short median lifetimes ($\sim 4 \times 10^7$ yr; Levison & Duncan 1997). They must be replenished from a longer-lived source if they are to maintain a steady state population: this source is now recognized in the Kuiper belt (Duncan et al. 1988). Published colors exist for only the brightest of the ~25 known Centaurs. We take the $V-R$ distribution for KBOs from Jewitt & Luu (2001) and for the Centaurs from Barucci et al. (2001) and Peixinho et al. (2001).

We also consider the color distribution for Jovian Trojans from Jewitt & Luu (1990). The Trojans are largely D-type and P-type objects, with low geometric albedos like those of the cometary nuclei. The $V-R$ distribution for a pure sample of D-types is taken from Fitzsimmons et al. (1994). While there is no established dynamical pathway from the Kuiper belt to the comets through the Jovian Trojans, it has sometimes been suggested that the Trojans might supply a fraction of the short-period comet population (Marzari, Farinella, & Vanzani 1995). In Table 5, we summarize parameters of the color distributions of other groups of objects.

4. RESULTS

The S'-distributions of the comets (Table 3) and KBOs are compared in Figure 1, where they are immediately seen to be different. For the nuclei, the mean gradient is $S' = 8.3\% \pm 2.8\%$ per 1000 Å (standard error on 12 objects), corresponding to $m_V - m_R = 0.45 \pm 0.02$. For the KBOs, the mean is $S' = 22.9\% \pm 1.7\%$ per 1000 Å (standard error on 28 objects), corresponding to $m_V - m_R = 0.61 \pm 0.01$. Figure 2 shows the cumulative distributions of S' for the two samples. The Kolmogorov-Smirnov test formally assesses the significance of the maximum difference between the two cumulative distributions. According to this test, the probability that the two distributions in Figures 1 and 2 are drawn from a single parent population is $P = 2.7 \times 10^{-4}$. The difference is therefore highly statistically significant, at the $1 - P = 99.97\%$ level of confidence. As another way to the same result, we note that none of the 12 cometary nuclei (neglecting 1P/Halley) is redder than the median, $S' = 25\%$ per 1000 Å, of the KBO colors. Since, by definition, 50% of the values in a distribution must lie above the median, we can conclude that the probability that the nucleus and KBO colors have the same median is $P \leq (\frac{1}{2})^{12} = 2.4 \times 10^{-4}$, similar to the result from the Kolmogorov-Smirnov test. The distribution of colors of the candidate dead comets is also different from the KBO distribution at a similar level of significance.

In short, inspection of Table 5 shows a substantial difference between the mean colors of the KBOs and Centaurs, on the one hand, and the cometary nuclei and the candidate

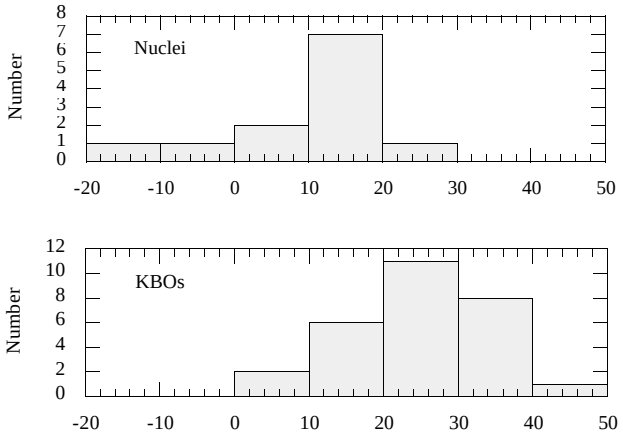

FIG. 1.—Distribution of the normalized reflectivity gradient, S' [% (1000 Å)$^{-1}$], for cometary nuclei (*top*) and KBOs (*bottom*).

dead comets, on the other (see also Fig. 3). For convenience, we define ultrared matter (URM) as having $S' > 25\%$ per 1000 Å, where the latter is the median S' of the KBOs. The URM is found only on the KBOs and Centaurs and is missing on the nuclei of active comets and the dead-comet candidates. Given that the KBOs, Centaurs, comets, and dead comets are related members of a single evolutionary dynamical sequence, this result is surprising. Here we consider possible explanations (the Trojans, which are not part of this sequence, are discussed separately in § 4.8).

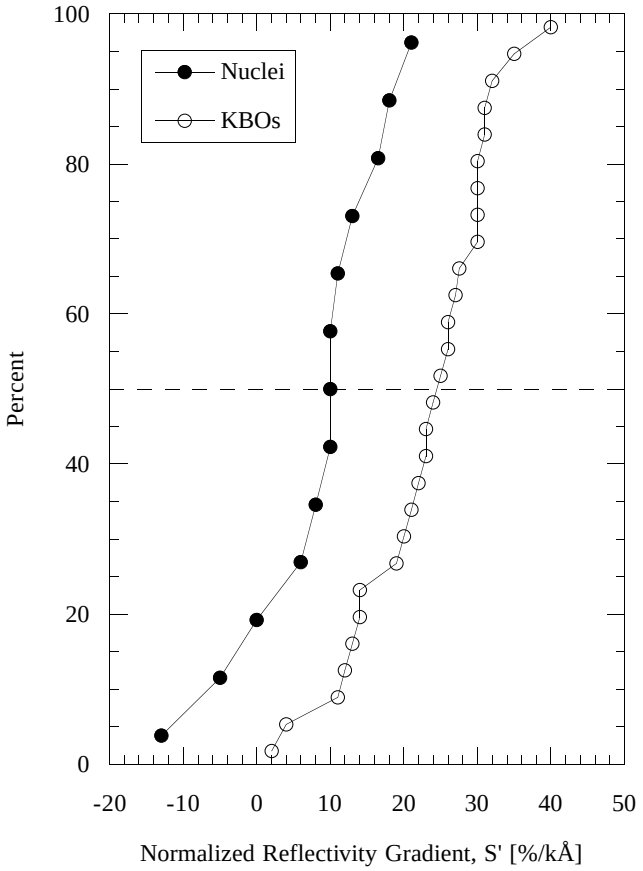

FIG. 2.—Cumulative distributions of S' for the cometary nuclei and KBOs.

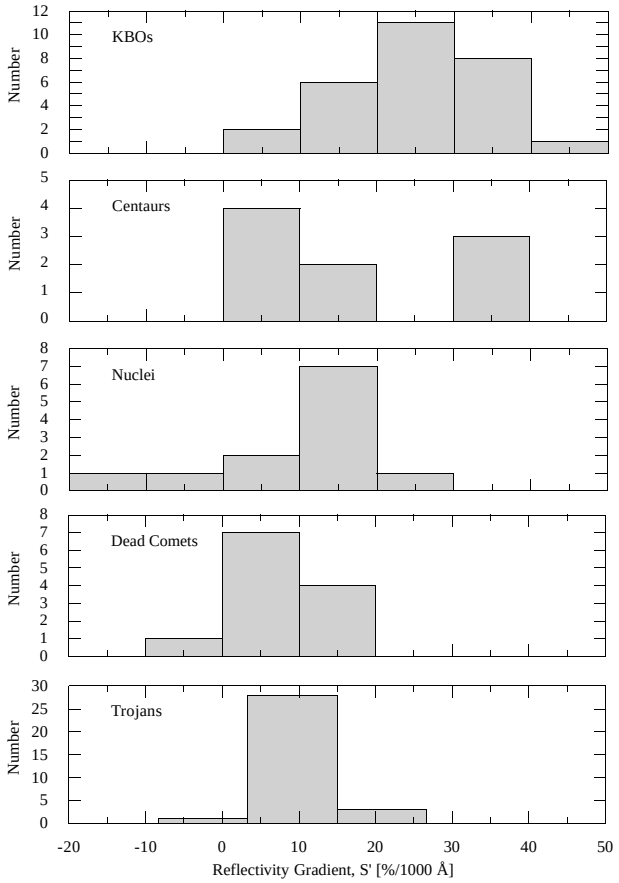

FIG. 3.—Histograms of the reflectivity gradient, S', for the different groups considered in § 3.

4.1. *Observational Error*

Perhaps the observational comparison between cometary nuclei and KBOs is compromised somehow. For example, might the cometary colors be contaminated by near-nucleus coma? We doubt this as a serious explanation of the color difference. First of all, we have selected objects in which coma contamination is minimal or absent. Our sample includes the least active objects still deserving of classification as comets. Even when coma has been detected, the spatial and photometric discrimination between the coma and nucleus appears secure. P/Tempel 2 is a good example. The nucleus was observed over a range of heliocentric distances, with and without resolved coma (Jewitt & Luu 1989). In all cases, consistent nuclear properties were measured. Near perihelion, when the coma was most obvious, the nucleus remained visible as a photometrically isolated, colorimetrically distinct feature of the comet. The nucleus rotational light curve, established prior to the appearance of coma, was also easily measured in the presence of coma. Clearly, contamination by the coma was not sufficient to obscure the signal from the nucleus even though P/Tempel 2 was one of the more active comets in our sample. Other well-observed comets, including the *HST* observations of nuclei, likewise clearly isolate a central signal from the nucleus. While it is possible to imagine scenarios in which the nuclear signal could be contaminated (because, for instance, of an orbiting or suborbital population of large grains), these scenarios seem arbitrary and contrived and are difficult to reconcile with the published body of measurements of nucleus rota-

tions and shapes (Jewitt & Meech 1988; Jewitt & Luu 1989; Meech & Belton 1990; Jewitt 1996; Lamy et al. 1998; Delahodde et al. 2001), sizes, and albedos (A'Hearn et al. 1989; Campins et al. 1987; Fernández et al. 2000; Millis et al. 1988).

It is known that the wavelength dependence of the scattering from a particulate surface is angle dependent, giving rise to a nonzero value of $dS'/d\alpha$. Since the cometary nuclei are, on the average, closer to the Sun than the KBOs, they are observed at systematically larger phase angles and are therefore more subject to the possible effects of phase reddening. We reject phase reddening as a significant source of the observed color difference for two reasons. First, the larger mean phase angles should cause the cometary nuclei to appear preferentially reddened, whereas they appear bluer, on average, than the KBOs. Second, the phase reddening coefficients are very small. Dahlgren et al. (1997) measured $dS'/d\alpha = 0.04\% \pm 0.03\%$ per 1000 Å per degree for D-type (low albedo) asteroids. At representative phase angles of 20° (Table 1), the expected reddening is only $\sim 0.8\% \pm 0.6\%$ per 1000 Å.

4.2. *Dynamical Error*

The most obvious possibility is that the nuclei are spectrally different from the KBOs because the comets are not derived from the Kuiper belt. It is true that the specific source region of the comets within the Kuiper belt has not been identified. Unstable regions near resonances are a plausible source, as are Plutinos destabilized by Pluto (Yu & Tremaine 1999), as are the scattered KBOs (Levison & Duncan 1997). Regardless of this ambiguity, however, the dynamical pathways from Kuiper belt to short-period comet seem so well established that we are reluctant to abandon the Kuiper belt–comet link.

4.3. *Restricted Source*

In principle, the comets might be derived from a limited region in the Kuiper belt within which surface colors differ from the mean color of all KBOs. For example, a localized source region could be lacking in the distinctive URM, consistent with the observed colors of the nuclei. The Centaurs provide a compelling argument against this "restricted-source hypothesis," since they display as wide a range of surface colors as the KBOs. In particular, the URM is unambiguously detected on Centaurs (5145) Pholus, (7066) Nessus, and 1999 UG_5 (Peixinho et al. 2001). Therefore, we reject the restricted-source hypothesis and infer that the URM is destroyed as the Centaurs become transformed into comets. This strongly suggests a thermal mechanism of destruction, driven by the rising surface equilibrium temperatures as the perihelia dip inside the orbit of Jupiter.

4.4. *Thermal Instability*

The observed color difference could result from thermal instability of the material responsible for the ultrared colors on the KBOs and Centaurs. If the URM were unstable at temperatures $\gtrsim 150$ K, for instance, it would be absent on the surfaces of all the cometary nuclei and dead-comet candidates in our sample. Instability could result from thermal dissociation of complex molecules responsible for the red colors, or from transformations between allotropes as seen in sulfur. In the absence of specific candidate materials, it is difficult to develop this hypothesis further, but we retain it as a possible explanation.

4.5. *Size Gradient*

The cometary nuclei have characteristic dimensions from a few to ~10 kilometers, whereas the well-measured KBOs are 100 km or larger in size. Therefore, the color difference between the nuclei and the KBOs could simply be an artifact of a color versus size trend among the KBOs. Such a trend could be created by collisions in the Kuiper belt. From particle-in-a-box–type calculations, it is easy to show that the collisional lifetime of KBOs in the classical belt is

$$\tau_c \sim 2.5 \times 10^9 [r/(1\ \mathrm{km})]\ . \quad (3)$$

Objects with $r \leq 2$ km have τ_c less than the age of the solar system. They are likely to be fragments produced in recent collisions (Farinella & Davis 1996) and may be shocked or otherwise thermally altered. Their mean cosmic-ray exposure ages will also be less than those of larger KBOs, for which disruptive collisions are improbable. The obvious test of this hypothesis is to search for evidence of a color versus size relation among objects in the Kuiper belt. No such relation is present in the existing data (Jewitt & Luu 2001, their Table 3). However, the well-observed KBOs are all much larger than the $r \sim 2$ km scale at which collisional effects become critical (eq. [3]). For this reason, the absence of a color versus size relation in existing data cannot be construed as significant evidence against the color versus size hypothesis. A 2 km radius KBO located at the distance of Neptune would have apparent red magnitude ~31. Measurement of the optical colors of such an object at useful (about ±5%) accuracy would be interesting but extremely challenging.

4.6. *Outgassing: Rubble Mantle*

A rubble mantle consists of debris blocks that are too large to be ejected from the surface of a sublimating body by gas drag forces. Mantles are observationally well established on the nuclei of short-period comets, where they act to stifle the flow of sublimated gases from all but restricted "active areas" (Hartmann, Tholen, & Cruikshank 1987; Rickman, Fernández, & Gustafson 1990; Jewitt 1992). Rubble mantles consist of material excavated from depth. Such material will have escaped the prolonged cosmic-ray bombardment received by the surface layers and therefore is expected to have different chemical and reflection properties. In the following, we use a highly simplified physical model that captures the essence of the resurfacing process. We do not attempt to model the process in fine detail, in part because the level of uncertainty regarding many of the key parameters is sufficient to prevent such an exercise.

The equation of motion of a dust grain embedded in the gas flow above a spherical, nonrotating nucleus is

$$m_d \frac{dv(r)}{dt} = C_D \pi a^2 \mu m_{\mathrm{H}} N_1(r)[v_g - v(r)]^2 - \frac{GM_n m_d}{r^2} \quad (4)$$

(see Whipple 1951), where m_d and M_n are the masses of the particle and the nucleus, respectively, μ is the molecular weight of the sublimated gas, v_g is its bulk velocity, m_{H} is the mass of the hydrogen atom, and $N_1(r)$ is the number density of the gas at radius r. The drag coefficient, C_D, is a dimensionless number of order unity. Also, $v(r)$ is the velocity of

the dust grain. We set $m_d = 4\pi\rho a^3/3$ and $m_n = 4\pi\rho r_n^3/3$ (ρ and ρ_n are the densities of the grain and the whole nucleus, respectively, and r_n is the radius of the nucleus) and define $a = a_c$ as the critical radius at which the left-hand side of equation (4) vanishes. Then

$$a_c \sim \frac{9C_D v_g}{16\pi G\rho\rho_n r_n}\frac{dm}{dt}, \tag{5}$$

where $dm/dt = \mu m_H N_1(r_n) v_g$ (kg m^{-2} s^{-1}) is, to within a numerical factor of order unity, the specific mass-loss rate due to sublimation. The numerical multipliers in equation (5) are artifacts of the assumed spherical shape of the nucleus and should not be accorded undue significance. The critical radius may be larger than given by equation (5) if the nucleus rotates, at least for particles located near the rotational equator. Nevertheless, the equation provides a useful estimate of the critical size for ejection. For example, consider a nucleus located at $R = 1$ AU with $\rho = \rho_n = 10^3$ kg m^{-3} and radius $r_n = 5 \times 10^3$ (m). We adopt $v_g = 500R^{-1/2}$ as an approximation to the outgassing velocity. Perfectly absorbing water ice in equilibrium sublimation at this distance has $dm/dt \sim 10^{-4}$ (kg m^{-2} s^{-1}). Substitution into equation (5) yields $a_c \sim 3 \times 10^{-2}$ (m) (3 cm). This is compatible with the detection of centimeter-sized particles in meteor streams associated with many short-period comets, and with 13 cm wavelength radar detections of large particles in comets. At distances R greater than 5 or 6 AU, $dm/dt \leq 10^{-10}$ kg m^{-2} s^{-1}, leading to $a_c \leq 10^{-7}$ (m). Such small particles are optically inefficient scatterers, explaining why water-driven dust comae are not observed around comets beyond Jupiter's orbit. Trans-Jovian comets, if active at all, are powered by the sublimation of carbon monoxide and (possibly) other supervolatiles (Senay & Jewitt 1994).

To provide thermal insulation and so to limit the flux of sublimated gases, the mantle thickness must approach the diurnal thermal skin depth, $L_D \sim (\kappa P_{\rm rot})^{1/2}$, where κ (m^2 s^{-1}) is the thermal diffusivity and $P_{\rm rot}$ (s) is the rotation period. For porous dielectrics likely to comprise the surface layers of comets and KBOs, we take $\kappa \sim 10^{-7}$ m^2 s^{-1}. With characteristic rotation period $P_{\rm rot} \sim 6$ hr, we obtain $L_D \sim 5$ cm. The timescale for growth of an insulating mantle is then

$$\tau_M \sim \frac{\rho_n L_D}{f_M\, dm/dt}, \tag{6}$$

where f_M is the fraction of the solid mass that cannot be ejected by gas drag. For an idealized size distribution in which the number of solid particles with radii in the range a to $a + da$ is $n(a)da = \Gamma a^{-q}\, da$ (Γ and q are constants), the fraction of the mass that is too large to be ejected by gas drag is

$$f_M = \frac{\int_{a_c}^{a_+} a^{3-q}\, da}{\int_{a_-}^{a_+} a^{3-q}\, da}, \tag{7}$$

where a_- and a_+ are the minimum and maximum particle sizes in the distribution. The cometary dust size distribution is best known in P/Halley, from in situ measurements by the *Giotto* and *Vega* spacecraft. The distribution is well measured in the 0.1 μm $\leq a \leq$ 100 μm range. It follows a modified power law, with $q \sim 4$ near $a = 100$ μm and becoming flatter at smaller sizes (Lamy, Grün, & Perrin 1987). In the spirit of the present model, we adopt $q = 4$ across the full range of particle sizes. Other values of q yield results qualitatively like those obtained here. In situ measurements of dust showed that the distribution extends down to $a_- = 10^{-8}$ m. The upper limit to the size of particles is less well determined. For definiteness, we take $a_+ = 10^{-1}$ m. With these assumptions, equation (7) gives

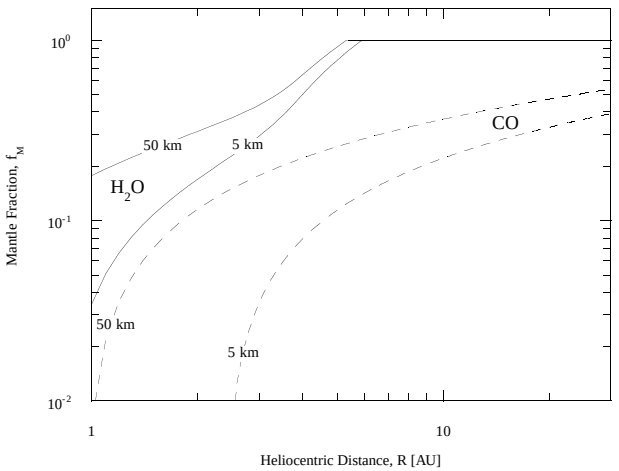

FIG. 4.—Mantle fraction (eq. [8]) as a function of heliocentric distance, for water ice and carbon monoxide sublimation. Nucleus radii are marked.

$$f_M = \frac{\ln(a_+/a_c)}{\ln(a_+/a_-)} \tag{8}$$

provided $a_+ \geq a_c$, and $f_M = 0$ otherwise. This function is shown in Figure 4, for two adopted values of the nucleus radius and for sublimating water and carbon monoxide ices. We have assumed $\rho = \rho_n = 10^3$ kg m^{-3} throughout. To calculate the sublimation mass flux, dm/dt, we solved the conservation of energy equation including terms for radiation and sublimation but neglecting thermal conduction (for simplicity). The figure shows that beyond $R \sim 6$ AU, the flux of sublimated water molecules is very weak and essentially no particles can be ejected by gas drag (i.e., $f_M = 1$). Close to the Sun, even large particles can be ejected, particularly from the smaller cometary nuclei, leading to small values of f_M. At $R < 2$ AU, CO is so volatile that no mantle can be held on the 5 km nucleus, and $f_M \sim 0$. The larger gravity of the 50 km nucleus can hold a few percent of the debris in a rubble mantle to $R \sim 1$ AU (Fig. 4).

Rubble mantle growth times (eq. [6]) are plotted against heliocentric distance in Figure 5. The mantle growth timescales for short-period comets with $R \leq 6$ AU are short compared with their median dynamical lifetimes ($\sim 4 \times 10^5$ yr; Levison & Duncan 1994). The prevalence of mantles on cometary nuclei is thus explained. For comparison, the dynamical transport time for Centaurs drifting inward from the Kuiper belt to be captured as short-period comets is $\sim 4 \times 10^7$ yr (Levison & Duncan 1997). Figure 5 shows that CO mantle growth timescales are shorter than this dynamical transport time. If the surfaces of Centaurs were rich in CO or other supervolatiles, this observation would mean that rubble mantles could form even before entry into the water-ice sublimation region. We consider it more likely that the surfaces of KBOs are depleted in supervolatiles even before entry into the gas-giant region of the solar system as Centaurs. This is because the supervolatile sublimation rate varies slowly with R ($dm/dt \propto R^{-2}$) and is still substantial in the $R \geq 30$ AU trans-Neptunian region. Therefore, we anticipate no global resurfacing of the Cen-

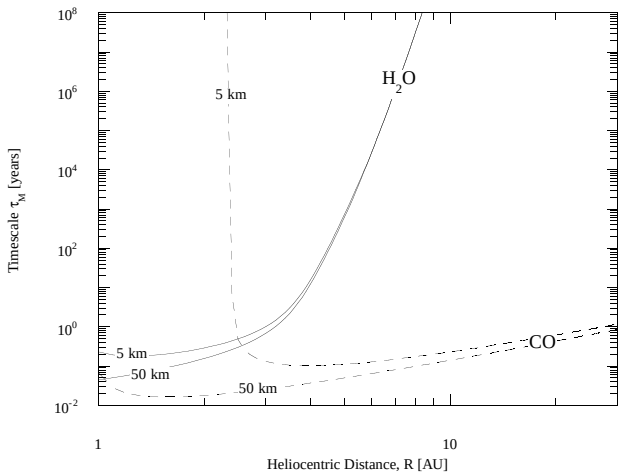

FIG. 5.—Timescales for rubble mantle growth produced by water and carbon monoxide sublimation, as a function of heliocentric distance. Nucleus radii are marked.

taurs by rubble mantles until these objects enter the water sublimation zone.

4.7. *Outgassing: Ballistic Mantle*

Resurfacing can occur via ballistic redeposition even on objects lacking widespread surface volatiles. Observations of anisotropic outgassing from Centaurs (2060) Chiron (Elliot et al. 1995) and P/Schwassmann-Wachmann 1 (Senay & Jewitt 1994) suggest that CO is exposed on only a fraction of the total surface area of these bodies. In the same way, mass loss is known to proceed from the cometary nuclei primarily by outgassing from "active areas" covering a small fraction of the surface. This suggests an alternate mode of resurfacing in which sublimation from limited areas of exposed surface volatiles leads to global burial of the original KBO surface under a layer of ballistically deposited debris. The formation of a "ballistic mantle" is distinct from the formation of a rubble mantle, since it can lead to complete resurfacing even on an object with a largely inert surface. In the present context, the ballistic mantle could be formed by a small exposure of volatile ice on an otherwise involatile surface composed of refractory, highly irradiated material.

The timescale to grow a ballistic mantle thick enough to inhibit heat conduction is

$$\tau_B \sim \frac{\rho_n L_D}{f_B \psi \, dm/dt}, \tag{9}$$

where L_D is again the thermal skin depth, f_B is the fraction of the solid matter launched into suborbital trajectories, and ψ is the fraction of the surface occupied by sublimating volatiles. In the short-period comets, this fraction is $10^{-3} \leq \psi \leq 0.1$. Obscuration of the original surface requires only a very thin layer of debris, perhaps only a few times the wavelength of light and certainly $\ll L_D$. Therefore, equation (9) provides a strong upper limit to the time needed to alter the surface reflection properties via a ballistic mantle.

We first estimate f_B. For any realistically broad size distribution, most of the solid material in the comet either will be too large to be launched by the local gas flow or, if sufficiently small, will be fully entrained in the gas flow and leave the nucleus at greater than the escape velocity. Only particles with velocities $0 \leq v \leq v_e$, where v_e is the gravitational escape velocity, can fall back. The fraction of the mass that may fall back is given by

$$f_B = \frac{\int_{a_e}^{a_c} a^{3-q}\, da}{\int_{a_-}^{a_+} a^{3-q}\, da}, \tag{10}$$

where a_e is the radius of the particle that can just reach escape velocity. We refer to f_B as the "capture fraction." With $q = 4$, equation (10) takes the simple form

$$f_B = \frac{\ln (a_c/a_e)}{\ln (a_+/a_-)} \tag{11}$$

The terminal velocity can be estimated from equation (4) as

$$v = v_g[1 - (a/a_c)^{1/2}] \, , \tag{12}$$

in which a_c is given by equation (5). By definition, $a = a_e$ when $v = v_e$. Therefore, by equation (12),

$$a_e/a_c = [1 - (v_e/v_g)]^2. \tag{13}$$

Substituting from equation (13) into equation (11), we obtain

$$f_B = \frac{\ln [1 - (v_e/v_g)]^{-2}}{\ln (a_+/a_-)}. \tag{14}$$

Figure 6 shows f_B as a function of R. The capture fraction is calculated from equation (14) using $a_- = 10^{-8}$ m, $a_+ = 10^{-1}$ m, and $v_g = 500R^{-1/2}$, which approximates the local thermal velocity in the gas. We adopt $\psi = 10^{-2}$. For small objects, $r \sim 5$ km, $f_B \sim 10^{-3}$. Larger objects, $r \sim 100$ km, have higher capture fractions, $f_B \sim 10^{-2}$, owing to their higher escape velocities.

Values of τ_B are plotted against heliocentric distance in Figure 7. We show models for two volatiles and two nucleus radii, corresponding to the typical short-period comets (radius $\sim$5 km) and larger Centaurs (radius $\sim$50 km). At a given heliocentric distance, τ_B is longer than τ_M by a factor of 10^2 to 10^3, but both timescales are short compared with the dynamical timescales for Centaurs and short-period comets. Thus, ballistic mantles may form on the surfaces of both Centaurs and short-period comets, if volatiles are

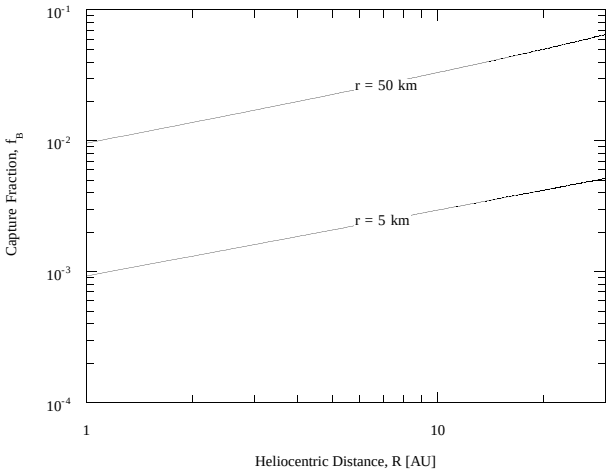

FIG. 6.—Capture fraction (eq. [14]) as a function of heliocentric distance for nucleus radii $r_n = 5$ km and $r_n = 50$ km, as marked.

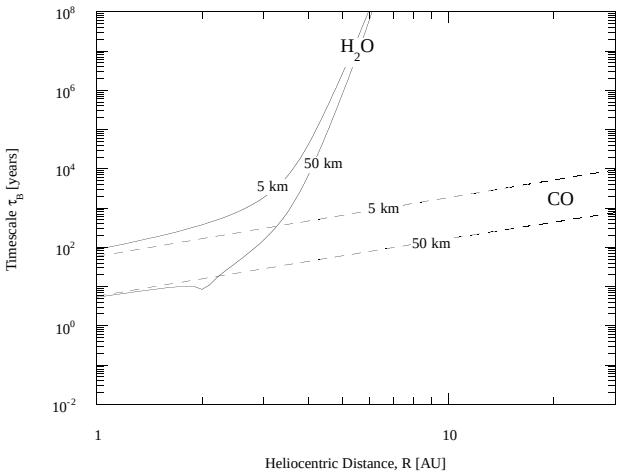

FIG. 7.—Timescales for ballistic mantle growth by water and carbon monoxide sublimation, as a function of heliocentric distance. Nucleus radii are marked.

exposed near the surfaces of these bodies. We believe that this process is ongoing in (2060) Chiron and P/Schwassmann-Wachmann 1, both of which are venting gas from localized active regions on the surface. The neutral colors of the surface of Chiron may result from resurfacing by a ballistically deposited mantle of debris. The surface colors of P/Schwassmann-Wachmann 1 have not yet been reliably measured.

4.8. *Trojans*

The mean color of the Jovian Trojan asteroids, $S'(\text{Trojans}) = 9.6\% \pm 0.9\%$ per 1000 Å ($n = 32$ objects; Jewitt & Luu 1990), closely matches that of the cometary nuclei (Fig. 3 and Table 5). Recent measurements of the Trojan population indicate that the Trojans are not likely to contribute more than about 10% to the flux of short-period comets (Jewitt, Trujillo, & Luu 2000), so the significance of this match might seem incidental. However, the Trojans formed at or beyond the snow line and may incorporate substantial amounts of water as ice. As seen from Figures 5 and 7, $\tau_M \sim 10^2$ yr and $\tau_B \sim 10^5$ yr at $R = 5$ AU. Ice in the Trojans could be trapped indefinitely by refractory mantles. Occasional collisions between Trojans might expose ice on the surfaces of these bodies, but the ice would sublimate and the mantles reseal on the timescale of τ_M. In many ways, the Trojans might be physically and compositionally similar to the comets, although derived from quite different regions of the Sun's accretion disk. Intriguing spectral similarities between comets and Trojans have been noted (Jewitt & Luu 1990). The two groups are also similar in having remarkably low albedos (Cruikshank 1977; A'Hearn et al. 1989; Campins et al. 1987; Millis et al. 1988; Fernández et al. 2001).

5. DISCUSSION

We have shown that mantle formation, either through the accumulation of classical lag deposits (§ 4.6) or by fallback of suborbital debris (§ 4.7), is a rapid and effective means of resurfacing. The existence of mantles is observationally well established on the nuclei of short-period comets. The primary evidence is the confinement of the products of outgassing to a series of jets overlying active areas on a fraction of the nucleus surface. Constriction of the mass loss by mantle formation may also help increase the effective sublimation lifetimes of the comets by factors $\psi^{-1} \sim 10^1$–10^3. This might help explain why dead comets do not outnumber their active counterparts (Fernández et al. 2001), as would be expected from the ratio of their respective lifetimes. The bulk of the mantling is driven by the sublimation of water ice.

Rubble mantle formation on the more distant (colder) Centaurs can result from the sublimation of supervolatiles such as CO. The 4.5 Gyr exposure ages of KBOs in the trans-Neptunian region will lead to the net depletion of CO and other supervolatiles from the surface layers of these objects even before they enter the region of the gas-giant planets. Therefore, we feel that most of the rubble mantling occurs when the incoming Centaurs cross Jupiter's orbit and become warm enough for water to sublimate. That this is not universally the case is shown by Centaurs (2060) Chiron and P/Schwassmann-Wachmann 1, both of which exhibit outgassing driven by limited exposures of near-surface supervolatiles. Chiron shows spectral evidence for water ice (Foster et al. 1999; Luu, Jewitt, & Trujillo 2000) that may have been ballistically deposited as grains launched by CO outgassing. Other Centaurs seem to retain their initial surfaces including some, such as (5415) Pholus, with irradiation mantles produced by long-term exposure in the Kuiper belt (Cruikshank et al. 1998).

Laboratory experiments with sublimating ice–refractory particle mixtures show color variations caused by restructuring that may well parallel the changes observed here (Stephens & Gustafson 1991). The muted colors (both slightly red and slightly blue) of these laboratory mantles are similar to the colors of the cometary nuclei and the candidate dead comets. The low geometric albedos (a few percent) of the laboratory mantles also resemble the albedos of the nuclei and dead comets.

While outgassing and resurfacing together constitute a sufficient process for burying any URM that may be exposed on the surfaces of incoming KBOs, other processes may independently act to remove the URM, as discussed above. We suspect, however, that the optical effects of resurfacing, once started, are overwhelming on all bodies where mass loss occurs. For example, even if the KBOs originally possess a color versus size gradient (§ 4.5), resurfacing will quickly reset the optical properties of the upper layers as soon as sublimation begins.

The present work suggests several promising avenues for observational follow-up. First, while finding URM on the nuclei is not precluded by the resurfacing models, these models predict that occurrences of URM should be rare. Observations to search for contrary evidence in the form of widespread URM on cometary nuclei are encouraged. Second, the effect of ballistic mantling on the Centaurs should be explored via careful measurements of their colors combined with sensitive searches for ongoing mass loss. The models indicate that URM should be found on a small fraction of outgassing Centaurs (given, roughly, by the ratio of τ_B to the dynamical transport time).

6. SUMMARY

1. The nuclei of comets are colorimetrically distinct from the Kuiper belt objects. The mean color of the nuclei is bluer than that of the KBOs, indicating a compositional and/or physical difference between these two groups.

2. Ultrared matter, defined as material having a spectral gradient $S' > 25\%$ per 1000 Å in the VR region of the spectrum, is present on some KBOs and Centaurs but is missing from the nuclei of short-period comets and candidate dead comets.

3. The KBOs, Centaurs, cometary nuclei, and candidate dead comets represent different stages of a single dynamical evolutionary sequence. The observations therefore require that the ultrared matter is destroyed or removed during the journey from Kuiper belt to inner solar system.

4. Resurfacing by sublimation constitutes a simple and natural explanation for the absence of ultrared matter on cometary nuclei. The timescale for burial of the original surface of an incoming cometary nucleus under a debris mantle is short compared with the dynamical transport time from the Kuiper belt to the inner solar system. Resurfacing is rapid (and, apparently, universal) once the objects enter the water sublimation zone ($R \leq 6$ AU).

We thank John Dvorak for operating the University of Hawaii telescope, and the anonymous referee for a prompt review. This work was supported by a grant to D. C. J. from NASA's Planetary Astronomy Program.

REFERENCES

A'Hearn, M. F., Campins, H., Schleicher, D. G., & Millis, R. L. 1989, ApJ, 347, 1155
Altenhoff, W. J., & Stumpff, P. 1995, A&A, 293, L41
Barucci, M. A., Fulchignoni, M., Birlan, M., Doressoundiram, A., Romon, J., & Boehnhardt, H. 2001, A&A, 371, 1150
Boehnhardt, H., Rainer, N., Birkle, K., & Schwehm, G. 1999, A&A, 341, 912
Campins, H., A'Hearn, M. F., & McFadden, L.-A. 1987, ApJ, 316, 847
Campins, H., Osip, D. J., Rieke, G. H., & Rieke, M. J. 1995, Planet. Space Sci., 43, 733
Campins, H., Telesco, C. M., Osip, D. J., Rieke, G. H., Rieke, M. J., & Schulz, B. 1994, AJ, 108, 2318
Chamberlin, A. B., McFadden, L.-A., Schulz, R., Schleicher, D. G., & Bus, S. J. 1996, Icarus, 119, 173
Cruikshank, D. P. 1977, Icarus, 30, 224
Cruikshank, D. P., et al. 1998, Icarus, 135, 389
Dahlgren, M., Lagerkvist, C.-I., Fitzsimmons, A., Williams, I. P., & Gordon, M. 1997, A&A, 323, 606
Davies, J. K., et al. 2001, Icarus, 150, 69
Delahodde, C. E., Meech, K. J., Hainaut, O. R., & Dotto, E. 2001, A&A, 376, 672
Duncan, M., Quinn, T., & Tremaine, S. 1988, ApJ, 328, L69
Elliot, J. L., et al. 1995, Nature, 373, 46
Farinella, P., & Davis, D. R. 1996, Science, 273, 938
Fay, T. D., & Wisniewski, W. 1978, Icarus, 34, 1
Fernández, J. A. 1980, MNRAS, 192, 481
Fernández, Y. R., Jewitt, D. C., & Sheppard, S. S. 2001, ApJ, 553, L197
Fernández, Y. R., et al. 2000, Icarus, 147, 145
Fitzsimmons, A., Dahlgren, M., Lagerkvist, C.-I., Magnusson, P., & Williams, I. P. 1994, A&A, 282, 634
Foster, M. J., Green, S. F., McBride, N., & Davies, J. K. 1999, Icarus, 141, 408
Hartmann, W. K., Tholen, D. J., & Cruikshank, D. P. 1987, Icarus, 69, 33
Hicks, M. D., Buratti, B. J., Newburn, R. L., Jr., & Rabinowitz, D. L. 2000, Icarus, 143, 354
Hicks, M. D., Fink, U., & Grundy, W. M. 1998, Icarus, 133, 69
Jewitt, D. 1996, Earth Moon Planets, 72, 185
Jewitt, D., & Danielson, G. E. 1984, Icarus, 60, 435
Jewitt, D., & Kalas, P. 1998, ApJ, 499, L103
Jewitt, D., & Luu, J. 1989, AJ, 97, 1766
Jewitt, D., & Meech, K. 1987, AJ, 93, 1542
Jewitt, D., & Meech, K. J. 1985, Icarus, 64, 329
Jewitt, D. C. 1992, in Observations and Physical Properties of Small Solar System Bodies, ed. A. Brahic, J.-C. Gérard, & J. Surdej (Liège: Inst. d'Astrophys., Univ. Liège), 85
Jewitt, D. C., & Luu, J. X. 1990, AJ, 100, 933
———. 2001, AJ, 122, 2099
Jewitt, D. C., & Meech, K. J. 1988, ApJ, 328, 974
Jewitt, D. C., Trujillo, C. A., & Luu, J. X. 2000, AJ, 120, 1140
Johnson, R. E., Cooper, J. F., Lanzerotti, L. J., & Strazzulla, G. 1987, A&A, 187, 889
Kamoun, P. G., Campbell, D. B., Ostro, S. J., Pettengill, G. H., & Shapiro, I. I. 1982, Science, 216, 293
Lamy, P. L., Grün, E., & Perrin, J. M. 1987, A&A, 187, 767
Lamy, P. L., Toth, I., A'Hearn, M. F., & Weaver, H. A. 1999, Icarus, 140, 424
Lamy, P. L., Toth, I., Jorda, L., Weaver, H. A., & A'Hearn, M. 1998, A&A, 335, L25
Landolt, A. U. 1992, AJ, 104, 340
Levison, H. F., & Duncan, M. J. 1994, Icarus, 108, 18
———. 1997, Icarus, 127, 13
Luu, J., & Jewitt, D. 1990a, Icarus, 86, 69
———. 1996, AJ, 112, 2310
Luu, J. X. 1993, Icarus, 104, 138
Luu, J. X., & Jewitt, D. C. 1990b, AJ, 99, 1985
———. 1990c, AJ, 100, 913
Luu, J. X., Jewitt, D. C., & Trujillo, C. 2000, ApJ, 531, L151
Marsden, B. G. 2000, IAU Circ. 7403
Marzari, F., Farinella, P., & Vanzani, V. 1995, A&A, 299, 267
Meech, K. J., & Belton, M. J. S. 1990, AJ, 100, 1323
Millis, R. L., A'Hearn, M. F., & Campins, H. 1988, ApJ, 324, 1194
Oort, J. H. 1950, Bull. Astron. Inst. Netherlands, 11, 91
Peixinho, N., Lacerda, P., Ortiz, J., Doressoundiram, A., Roos-Serote, M., & Gutiérrez, P. J. 2001, A&A, 371, 753
Rickman, H., Fernández, J. A., & Gustafson, B. Å. S. 1990, A&A, 237, 524
Senay, M. C., & Jewitt, D. 1994, Nature, 371, 229
Stephens, J. R., & Gustafson, B. Å. S. 1991, Icarus, 94, 209
Tegler, S. C., & Romanishin, W. 2000, Nature, 407, 979
Thomas, N., & Keller, H. U. 1989, A&A, 213, 487
Whipple, F. L. 1951, ApJ, 113, 464
Wilson, P. D., Sagan, C., & Thompson, W. R. 1994, Icarus, 107, 288
Yu, Q., & Tremaine, S. 1999, AJ, 118, 1873